



City Research Online

City, University of London Institutional Repository

Citation: White, M. & Sayma, A. I. (2015). The impact of component performance on the overall cycle performance of small-scale low temperature organic Rankine cycles. IOP Conference Series: Materials Science and Engineering, 90(1), 012063. doi: 10.1088/1757-899x/90/1/012063

This is the accepted version of the paper.

This version of the publication may differ from the final published version.

Permanent repository link: <https://openaccess.city.ac.uk/id/eprint/13380/>

Link to published version: <https://doi.org/10.1088/1757-899x/90/1/012063>

Copyright: City Research Online aims to make research outputs of City, University of London available to a wider audience. Copyright and Moral Rights remain with the author(s) and/or copyright holders. URLs from City Research Online may be freely distributed and linked to.

Reuse: Copies of full items can be used for personal research or study, educational, or not-for-profit purposes without prior permission or charge. Provided that the authors, title and full bibliographic details are credited, a hyperlink and/or URL is given for the original metadata page and the content is not changed in any way.

City Research Online:

<http://openaccess.city.ac.uk/>

publications@city.ac.uk

The impact of component performance on the overall cycle performance of small-scale low temperature organic Rankine cycles

M White and A I Sayma

School of Mathematics, Computer Science and Engineering, City University London, UK.

Email: Martin.White.1@city.ac.uk

Abstract. Low temperature organic Rankine cycles offer a promising technology for the generation of power from low temperature heat sources. Small-scale systems (~10kW) are of significant interest, however there is a current lack of commercially viable expanders. For a potential expander to be economically viable for small-scale applications it is reasonable to assume that the same expander must have the ability to be implemented within a number of different ORC applications. It is therefore important to design and optimise the cycle considering the component performance, most notably the expander, both at different thermodynamic conditions, and using alternative organic fluids. This paper demonstrates a novel modelling methodology that combines a previously generated turbine performance map with cycle analysis to establish at what heat source conditions optimal system performance can be achieved using an existing turbine design. The results obtained show that the same turbine can be effectively utilised within a number of different ORC applications by changing the working fluid. By selecting suitable working fluids, this turbine can be used to convert pressurised hot water at temperatures between 360K and 400K, and mass flow rates between 0.45kg/s and 2.7kg/s, into useful power with outputs between 1.5kW and 27kW. This is a significant result since it allows the same turbine to be implemented into a variety of applications, improving the economy of scale. This work has also confirmed the suitability of the candidate turbine for a range of low temperature ORC applications.

1. Nomenclature

a	Speed of sound, m/s
D	Rotor diameter, m
h	Enthalpy, J/kg
\dot{m}	Mass flow rate, kg/s
N	Rotational speed, RPM
P	Pressure, kPa
PP	Pinch point
PR	Pressure ratio
\dot{Q}	Heat input, J/s
s	Entropy, J/(kg K)
T	Temperature, K
\dot{W}	Power, J/s
η	Isentropic efficiency, %
μ	Viscosity, Pa s
ρ	Density, kg/m ³

Δh_s	Turbine isentropic enthalpy drop, J/kg
ΔT_{sh}	Degree of superheat, K

Subscripts

1-4	ORC locations
c	Cold source
ci	Cold source inlet
cp	Cold source pinch point
e	Expander
h	Heat source
hi	Heat source inlet
hp	Heat source pinch point
n	Net work
o	ORC
p	Pump
s	After isentropic compression/expansion
'	Saturated conditions

2. Introduction

The organic Rankine cycle (ORC) is a promising technology for the sustainable generation of power from a number of different heat sources such as solar energy, biomass, geothermal and waste heat. These applications cover an array of heat source temperatures ranging anywhere from 80°C to 300°C, whilst power outputs range from few kilowatts up to few megawatts. At present ORC technology has been successfully commercialised for large-scale applications [1,2]. For small scale applications the economy of scale and technical challenges such as the development of an efficient and economical expander restrict large scale implementation of the technology, although bespoke systems are available on the market [3,4]. However, if these challenges can be overcome the implementation of small scale ORCs will be an interesting technology offering sustainable, localised power generation.

Typically ORCs are characterised by the heat source temperature, and this significantly affects the thermodynamic cycle and expander design. High temperature heat sources such as exhaust gases from internal combustion engines require very high pressure ratios, which can only be achieved by a turbo-expander such as those presented in [5,6]. The relatively small enthalpy drop of organic fluids permits these pressure ratios to be achieved over a single stage, but at the expense of introducing supersonic flows within the stator and rotor passages. Comparatively, low temperature applications have lower pressure ratios, permitting the use of volumetric expanders, such as screw and scroll machines. However these expanders are typically obtained by the reverse operation of existing compressors, and therefore the achievable efficiency may be limited [7,8]. Furthermore, at the target power of 10kW, screw expanders experience high leakage flows [9], whilst scrolls are yet to be proven [10]. For a 10kW ORC utilising a low temperature heat source (100-120°C), the authors believe an efficient radial turbine would be the most suitable expander choice.

Thermodynamic cycle design and working fluid selection remain critical aspects of ORC, and this is highlighted by the abundance of research available on the topic [11-13]. Furthermore, due to the large number of interdependencies, the implementation of a suitable optimisation algorithm to arrive at an optimal system is essential [14-16]. At this point, it is important to make the distinction between two types of cycle design. The first type of design comprises of designing an optimal system for a particular application, allowing the thermodynamic cycle to be optimised assuming that each component performs at its design point. This simplifies the turbine modeling since the target efficiency can be specified; the turbine will then be effectively designed to achieve this. However, this approach may lead to a high cost, bespoke system that may not be economical to implement.

By comparison, the second type of cycle design considers optimising a group of existing components to generate the maximum power from a specified heat source. From the point of view of economic feasibility this may be beneficial for small-scale systems since the key component, the turbine, can be manufactured on a relatively large scale and then implemented into a range of different applications. For this second type of cycle design it is important to couple component models with cycle analysis to account for component off-design performance. In this instance the search for optimal cycle conditions may move the expander performance away from design conditions. Therefore it is critical to be able to accurately predict how the expander may perform, and the impact that operating at off-design will have on the cycle performance. At present, the assumption of constant turbine efficiency is a shortcoming within many thermodynamic papers.

The performance of a turbine is generally characterised by means of a turbine performance map plotting mass flow rate and efficiency as functions of pressure ratio and rotational speed. Similitude theory is then used to non-dimensionalise this map. Similitude theory has been successfully validated and is widely applied to ideal gases such as air [17]. With care it can also be used to estimate the performance following a change in working fluid, so long as the thermodynamic properties of the two fluids are not significantly different [18]. The application of similitude theory to ORC turbines has been considered by a number of authors [19-21]. However, this is often with reference to simplified non-dimensional parameters, which are only applicable to ideal gases. Until recent preliminary work published in the literature, the suitability of applying similitude theory to real gases such as organic fluids found within ORCs had not been investigated or validated.

Previous work has led to the thermodynamic design and optimisation of a candidate ORC turbine [22,23]. The turbine performance at the design point has been validated using CFD, and the resulting performance map has been constructed. This paper demonstrates a modeling methodology that combines the validated turbine map with cycle analysis in a bid to establish the range of heat source conditions that can be converted into useful power using this candidate turbine. Through doing this, the aim of this paper is to confirm the suitability of implementing this existing design into a number of different ORC applications. Not only will this further validate this candidate turbine design, but it may also show how the economy of scale of small-scale ORC turbines can be improved by implementing the same turbine into a number of applications by changing the working fluid and cycle design parameters according to the heat source available.

Within this paper the details for the turbine and ORC models are summarised before the modeling methodology is demonstrated considering a test case. Having shown how the model can be used to obtain the optimal operating point for a given heat source temperature and working fluid, the model is ran for a range of heat source temperatures and working fluids and the range of potential applications for this candidate turbine is established.

3. Turbine modelling

3.1 Similitude theory

The performance of a turbomachine can be described by the isentropic enthalpy change across the turbine Δh_s , the power output \dot{W}_e , and the isentropic efficiency η_e . These parameters are a function of the turbine diameter D , rotational speed N , mass flow rate \dot{m}_0 , and the fluid stagnation speed of sound a_3 , and density ρ_3 at the turbine inlet. Dimensional analysis reduces these parameters to a number of non-dimensional groups (Equation 1). The parameters on the left hand side are referred to as the head coefficient, isentropic efficiency and power coefficient respectively. The first term on the right hand side is the flow coefficient, the second is the Reynolds number and the third term is the blade Mach number.

$$\left[\frac{\Delta h_s}{N^2 D^2}, \eta_e, \frac{\dot{W}_e}{\rho_3 N^3 D^5} \right] = f \left\{ \frac{\dot{m}_o}{\rho_3 N D^3}, \frac{\rho_3 N D^2}{\mu}, \frac{N D}{a_3} \right\} \quad (1)$$

After obtaining performance data for a given working fluid at particular inlet conditions, the non-dimensional parameters can be calculated and the non-dimensional performance map constructed. Typically, for ideal gas applications the effect of Reynolds number is small and may be neglected [17]. In this instance a performance map describes how the flow coefficient and isentropic efficiency vary with changes in the head coefficient and blade Mach number. For changes in working fluid or turbine inlet conditions, it is assumed that the same values for the head coefficient, isentropic efficiency and power coefficient are obtained when the flow coefficient and blade Mach number remain constant. It is then a simple matter to determine the new performance data.

Preliminary analysis undertaken has shown that the same non-dimensional scaling laws may only be applied to real gases when the deviation in Reynolds number is not significant. This conclusion was obtained after comparing predictions made by the scaled performance map to those obtained using CFD. It was found that the predictions agreed with the CFD results to within +/- 2% when the deviation in Reynolds number was between -75% and +75%. At deviations higher than +75%, it was found that accurate predictions were only made at subsonic conditions, at mass flow rates smaller than the choking mass flow rate. These results were found to hold true for different fluids, in addition to changes in the turbine inlet conditions. Combining the Reynolds number and blade Mach number results in an additional expression that relates only the thermodynamic properties (Equation 2). Provided that the same blade Mach number is maintained, this expression may be used to determine whether the deviation in Reynolds number is within the specified range.

$$\left(\frac{\rho_3 a_3}{\mu_3} \right)_A = \left(\frac{\rho_3 a_3}{\mu_3} \right)_B \quad (2)$$

3.2 Candidate ORC turbine and performance map

Previous work has considered the thermodynamic analysis of a suitable low temperature ORC [22], and this has led to the design of a candidate radial turbine operating with R245fa [23]. The thermodynamic specification and the design point operation parameters for the turbine are summarised in Table 1. The data points required to construct the performance map data points were obtained using CFD, and these results were then curve fitted to generate the turbine performance maps shown in Figures 1 and 2. Within the CFD real gas properties were accounted for by generating gas property tables using REFPROP; this is a program consisting of state-of-the-art equations of state for a large array of working fluids [24]. In Figure 1 and 2 the non-dimensional parameters in Equation 1 have been reduced to the head coefficient ($\Delta h_s/a_3^2$), the flow coefficient ($\dot{m}_o/\rho_3 a_3$) and the rotational speed (N/a_3). This can be done since the diameter of the turbine does not change, although it should be noted that these parameters are no longer non-dimensional. The reduced rotational speeds considered range from 50% to 125% of the design value. Although operation at these extreme rotational speeds may be too far from the normal turbine operating point to be feasible, these speeds have been selected to extend the operating envelope for the purposes of analysis only. After completing the analysis the rotational speed should be verified to ensure it lies within a feasible range.

The range of applicability for the developed turbine map is established in Figure 3. The relationship described by Equation 2 has been plotted over a range of turbine inlet temperatures and pressures. This clearly demonstrates that this turbine, operating with R245fa, is suitable for ORC applications with turbine inlet temperatures between approximately 315K and 375K.

Table 1. Thermodynamic conditions and design specification for the developed ORC turbine.

Working Fluid	-	R245fa	[-]
Total Inlet Temperature	T_3	350.00	[K]
Total Inlet Pressure	P_3	623.06	[kPa]
Mass Flow Rate	\dot{m}_o	0.70	[kg/s]
Pressure Ratio	PR	2.50	[-]
Isentropic Efficiency	η_e	85.00	[%]
Power Output	\dot{W}_e	10.22	[kW]
Rotational Speed	N	37,525	[RPM]
Rotor Diameter	D	66.68	[mm]

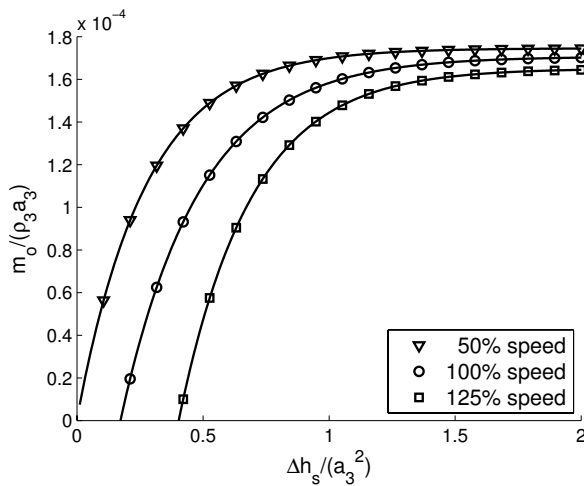


Figure 1. Variation of flow coefficient with head coefficient at 50%, 100% and 125% of the design blade Mach number.

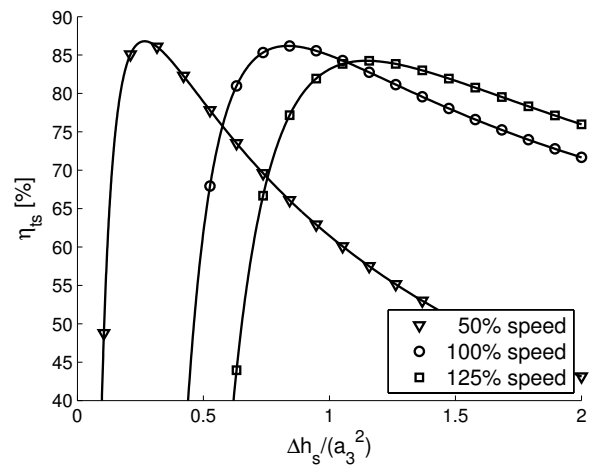


Figure 2. Variation in isentropic efficiency with head coefficient at 50%, 100% and 125% of the design blade Mach number.

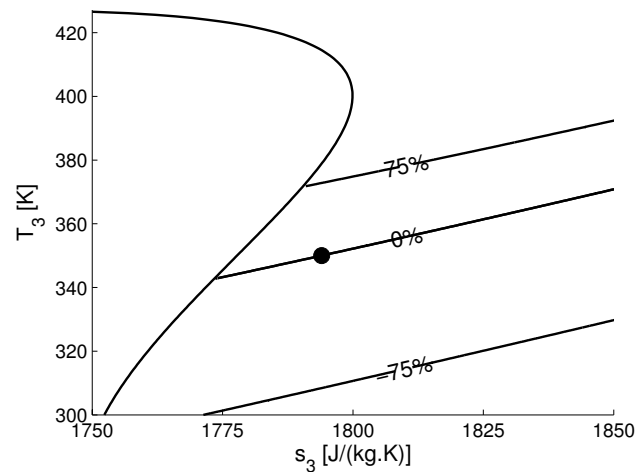


Figure 3. Deviation in Reynolds number with variations in turbine total inlet conditions for R245fa assuming that the blade Mach number has been conserved (the dot represents conditions at the turbine design point).

4. ORC modelling

To analyse the suitability of implementing the developed turbine to a number of different ORC applications, a thermodynamic model has been developed that establishes the range of heat source conditions that can effectively be converted into useful power. Since the main focus of this work is the turbine, it was deemed suitable to model a simple subcritical ORC without a regenerator. Not only does this simplify the analysis, but it was also considered an advantage in terms easing manufacture and reducing the overall cost of the system.

The complete thermodynamic analysis of the ORC is well covered within many research papers [11-13], so the model will only be summarised here. The simple ORC model has been linked with REFPROP for real fluid properties. The T-s diagram for the ORC is shown in Figure 4, along with the notation used throughout this paper.

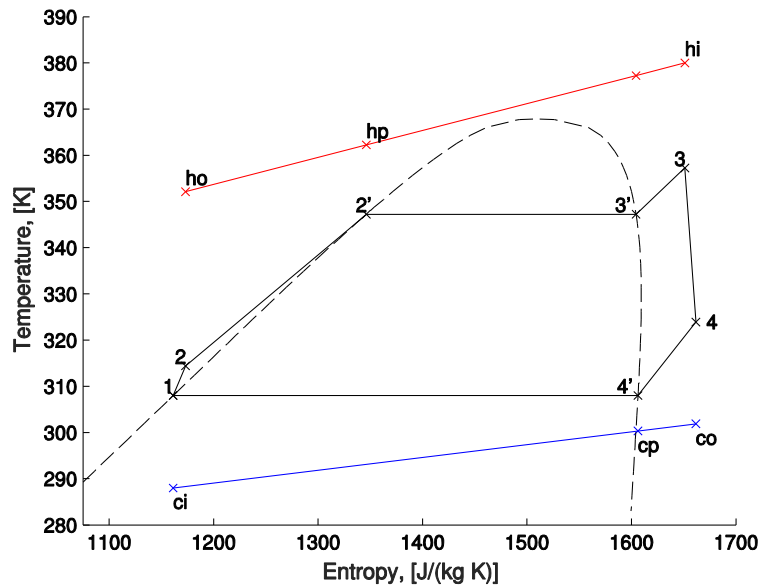


Figure 4. Typical T-s diagram for the simple subcritical low temperature ORC.

Assuming that the working fluid enters the pump as a saturated liquid all thermodynamic properties at the pump inlet are determined by the input condensation temperature T_1 . The pump outlet conditions are then specified by the input ORC pressure ratio PR, and isentropic pump efficiency η_p .

$$h_2 = h_1 + \frac{h_{2s} - h_1}{\eta_p} \quad (3)$$

Neglecting pressure drops through the evaporator the working fluid properties at locations 2' (saturated liquid) and 3' (saturated vapour) are also known whilst an input value for the amount of superheat ΔT_{sh} , and evaporator pinch point PP_h then provide the ORC conditions at the evaporator outlet (3), and the heat source conditions at the pinch point (hp) respectively. An energy balance then provides the ratio of working fluid mass flow rate \dot{m}_o , to the heat source mass flow rate \dot{m}_h .

$$\frac{\dot{m}_o}{\dot{m}_h} = \frac{h_{hi} - h_{hp}}{h_3 - h_{2'}} \quad (4)$$

For the specified ORC cycle conditions the isentropic enthalpy drop across the turbine, and therefore the reduced head coefficient ($\Delta h_s/a_3^2$) can now be established. Using Figure 1 this supplies the minimum and maximum flow coefficients, which correspond to 125% and 50% of the design non-dimensional rotational speed respectively. From this the physical limits for the working fluid mass flow rate are easily obtained. An array of mass flow rates ranging from the minimum to the maximum is then constructed and for each mass flow rate the flow coefficient is calculated and the reduced rotational speed is obtained through interpolation of Figure 1. Similarly, the reduced head coefficient and reduced rotational speed supplies the turbine isentropic efficiency η_e for each flow coefficient through interpolation of Figure 2. The deviation in Equation 2 from the value associated with the details in Table 1 is also calculated, to ensure that it lies within the -75% and +75% limits. After this, the working fluid properties at the turbine outlet are then determined using Equation 5. The heat source mass flow rate also follows from Equation 4. The result of this is that for a specified thermodynamic ORC cycle, there is a range of mass flow rates that can be achieved each with a different turbine isentropic efficiency.

$$h_4 = h_3 - \eta_e(h_3 - h_{4s}) \quad (5)$$

An energy balance within the condenser completes the cycle analysis. Again, neglecting pressure drops the working fluid properties at 4' (saturated vapour) are known, whilst the condenser pinch point PP_c supplies the heat sink properties at the pinch point (cp). An energy balance then provides the required heat sink flow rate \dot{m}_c (Equation 6). Having completed the cycle analysis, the performance of the cycle is assessed in terms of the net power produced \dot{W}_n , and the cycle efficiency η_o (Equation 7).

$$\dot{m}_c = \frac{\dot{m}_o(h_{4'} - h_1)}{h_{ci} - h_{cp}} \quad (6)$$

$$\eta_o = \frac{\dot{W}_n}{\dot{Q}} = \frac{\dot{W}_e - \dot{W}_p}{h_3 - h_2} = \frac{(h_3 - h_4) - (h_2 - h_1)}{h_3 - h_2} \quad (7)$$

In addition to assessing the cycle performance, an additional parameters has been introduced that compares the net power to the maximum net power that could be produced using the same heat source with a turbine operating at an optimal efficiency of 85%. For fixed values of T_1 , ΔT_{sh} , PP_e , with a fixed heat source temperature and mass flow rate, there exists an optimal pressure ratio at which optimal power can be produced. The top graph in Figure 5 shows this optimal pressure ratio, and corresponding maximum power for a range of heat sources with a fixed mass flow rate of 1.0kg/s. The bottom graph shows that for a fixed temperature, the optimal pressure ratio remains fixed, although the net power increases linearly with mass flow rate. Therefore using the input heat source temperature and the heat source flow rate calculated using Equation 4, and assuming T_1 , ΔT_{sh} and PP_e remain constant, the maximum potential power can be obtained using Figure 5. It should be noted that for this maximum a turbine efficiency of 85% has been selected since this was considered to be an achievable target for design point efficiency. When comparing the actual net power to the maximum power, if the actual power is greater, this is the result of the turbine actually operating at a slightly higher efficiency than 85%.

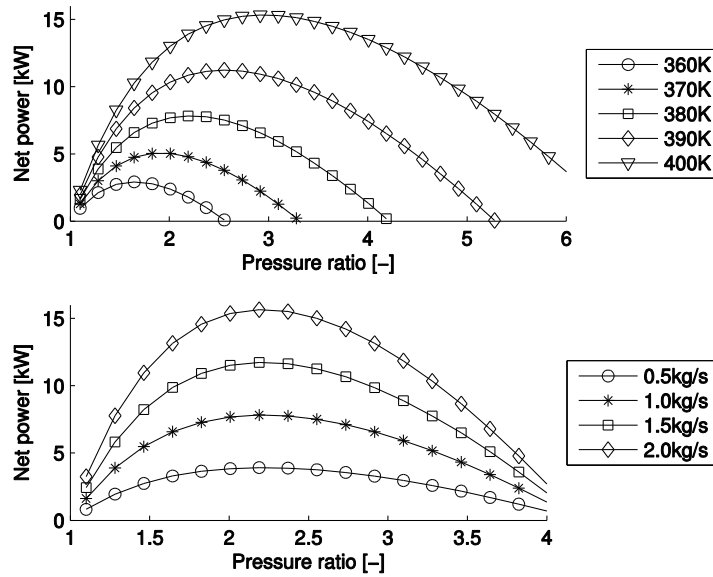


Figure 5. Variation in net power produced as a function of pressure ratio for different heat source conditions. Top: fixed heat source mass flow rate of 1.0kg/s; Bottom: fixed heat source temperature of 380K.

5. Results and discussion

To first demonstrate the ORC modelling methodology, the operation of the turbine has been considered for a heat source temperature consisting of pressurised water at 380K and 400kPa, whilst the ORC working fluid is R245fa. Throughout this paper, the values for T_1 , PP_c , PP_e , ΔT_{sh} and η_p have all been fixed. This is because the focus here is on the turbine performance so the impact of variations in the pump and heat exchanger performance, although important, have been neglected. T_1 and PP_c largely dictate the required condenser area and the heat sink mass flow rate. The heat sink temperature is estimated to be 288K, whilst values of $T_1 = 313K$ and $PP_c = 10K$ have been selected which corresponds to an approximate 15K rise in the heat sink temperature through the condenser. The value for PP_e has been estimated to be 15K; both the evaporator and the condenser pinch points dictate the size of the heat exchangers, and represent a trade-off between performance and cost. The values selected have been found to provide a reasonable balance between these two aspects. It has been widely shown in the literature that superheating is not necessary for organic fluids since expansion from saturated vapour generally ends in the superheated region due to the slope of the saturated vapour curve. Therefore a small value of 2K has been selected just to ensure that the fluid is fully vaporised before entry into the turbine. Since the pump work is much smaller than the turbine work the impact of variations in pump efficiency are expected to be negligible; therefore the pump efficiency is assumed to be constant at 70%.

Using these fixed inputs the methodology outlined in Section 4 was implemented for a range of pressure ratios, with a range of possible working fluid mass flow rates being established at each pressure ratio. The result is a performance map that shows how the net power produced (as a percentage of the maximum potential power) varies with pressure ratio and ORC working fluid mass flow rate (Figure 6). The black lines indicate the heat source mass flow rate in kg/s. This figure is useful in that for a specified heat source at a known temperature and mass flow rate it is easy to assess the feasibility of using the given turbine. For example, if the heat source mass flow rate is close to 1.0kg/s, it is easy to see that at a pressure ratio of approximately 2.2 the turbine efficiency is high and 100% of the maximum potential net power that could be produced using this heat source can be

achieved by the cycle. However as the mass flow rate increases or decreases, the performance of the turbine deteriorates leading to a lower percentage of the maximum potential power being produced. For these heat source mass flow rates an alternative turbine may offer better performance, and further analysis would be required to establish whether the improved performance would be worth the increased costs associated with implementing a different design. None the less, it appears that for a heat source of 380K with a mass flow rate between 0.7kg/s and 1.2kg/s a reasonable performance can be achieved with this existing design operating with R245fa. For these flow rates the net power produced should remain above 90% of the maximum potential power.

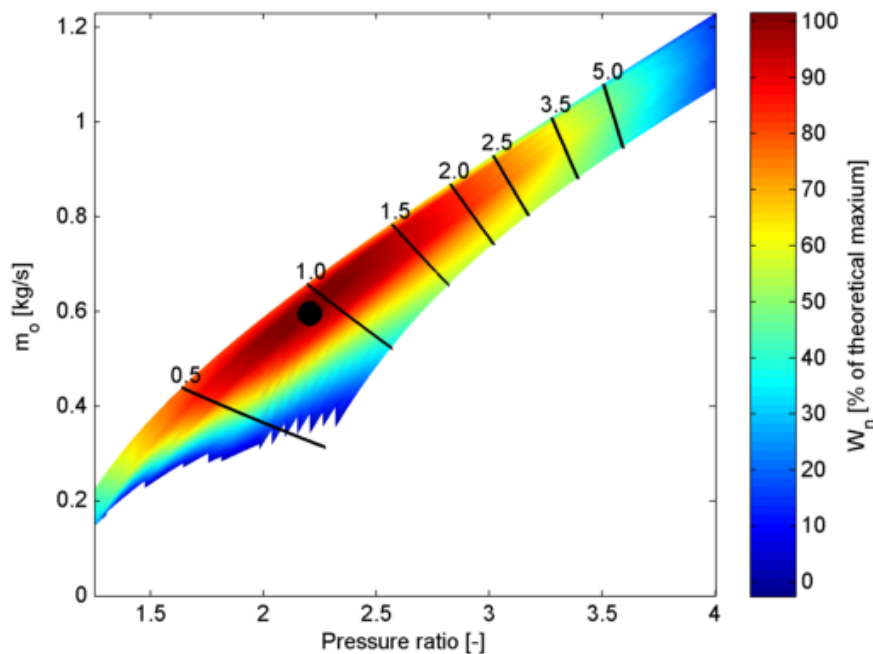


Figure 6. Contour of the net power produced by an ORC operating with the candidate turbine as a percentage of the maximum potential power. Heat source of water at 380K, and R245fa as working fluid. The black lines indicate the heat source mass flow rate in kg/s, whilst the black dot represents the point of optimal operation.

Having demonstrated the modelling methodology it is now suitable to extend the analysis to provide more useful results. Figure 6 only applies at one heat source temperature, and for one working fluid. Therefore the same method has been completed at three different heat source temperatures and for a variety of working fluids. The intention is that at each combination of heat source temperature and working fluid the optimal operating point can be determined. Referring to Figure 6, the optimal operating point for that particular setup has been shown as black dot. This is the point at which the net power produced is the highest percentage of the maximum potential power. Therefore, by completing this analysis the optimal heat source mass flow rate for a given combination of heat source temperature and working fluid will be established. Through doing this the range of heat sources that can be effectively converted into useful power using this turbine will therefore also be established.

The three heat source temperatures selected for this study are 360K, 380K and 400K. These temperatures were considered to span the range that could be effectively converted into power using this turbine. Below 360K the cycle efficiency would reduce significantly impacting the economic feasibility of such a system. In comparison, above 400K the pressure ratio increases, increasing the likelihood of supersonic flows. For these applications it would be more suitable to implement a turbine

specifically designed for supersonic operation. An initial review of screening studies resulted in 50 potential fluids. However, after considering suitable operating conditions, the evaporation and condensation pressures were estimated. Fluids with sub-atmospheric condensation pressures or supercritical evaporation pressures were neglected. Common refrigerant mixtures were neglected as these were found to have high saturation pressures, near critical evaporator pressures or negative gradient saturated vapour domes. The values for T_1 , PP_c , PP_e , ΔT_{sh} and η_p were again fixed, and the simulation model was run for each heat source temperature and working fluid. The optimal operating point for each combination of heat source temperature and mass flow rate was established and the resulting heat source mass flow rates and net powers produced are shown in Figure 7.

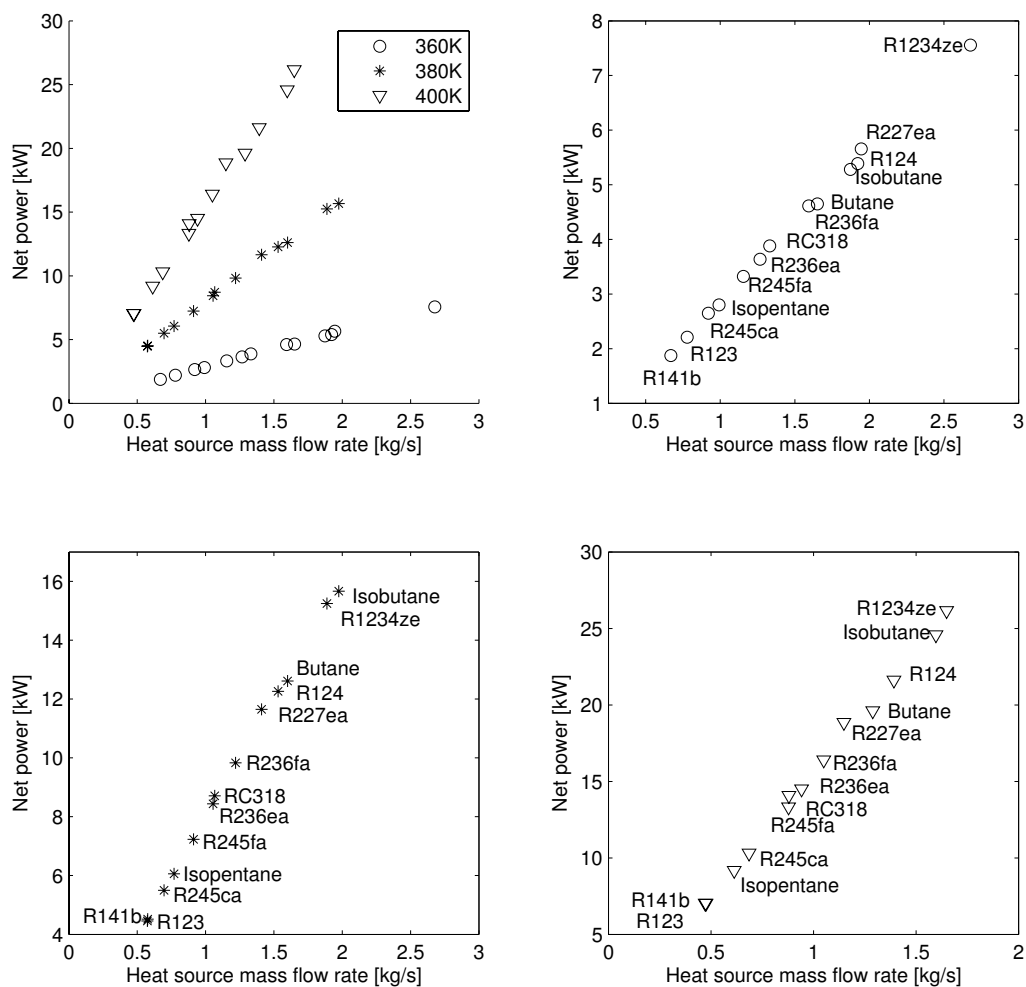


Figure 7. Cycle analysis results showing the heat source mass flow rates that can be accommodated by an ORC utilising the candidate turbine at each combination of heat source temperature and working fluid. Top left: summary of all results; top right: 360K; bottom left; 380K; bottom right; 400K.

The top-right graph in Figure 7 displays all of the simulation results, with each marker representing the result obtained for a particular working fluid at the respective heat source temperature. The remaining graphs expand these results, showing which working fluid each marker represents. The most striking observation is the large spread of heat source mass flow rates that be effectively

accommodated by using this turbine. For example, for a heat source temperature of 400K the same turbine can effectively convert a heat source ranging from 0.47kg/s to 1.65kg/s by simply changing the working fluid that operates within the cycle. The resulting power output ranges from 7.03kW up to 26.16kW. It should also be pointed out that across all of the operating points shown in Figure 7, the location of the optimal point (as previously described in Figure 6) is consistently close to 100% of the maximum potential power, with a corresponding turbine isentropic efficiency close to 85%. This confirms that at the corresponding heat source conditions, the ORC is operating at the optimal pressure ratio, and that this pressure ratio corresponds to the optimal head coefficient for the candidate turbine. In other words, for the same heat source conditions it would be unlikely that designing a new turbine would offer much improvement on the turbine, and therefore cycle, performance.

In terms of the turbine rotational speed it is interesting to note that as the heat source temperature increases, the non-dimensional speed at which optimal performance is obtained also increases. For a heat source temperature of 360K, all of the optimal points in Figure 7 correspond to non-dimensional rotational speeds between 60% and 80% of the design value. For the 380K and 400K cases this increases to between 80% and 100%, and 100% and 120% of the design speed respectively. This suggests that below 360K and above 400K, the non-dimensional speed would move outside practical limits for this turbine, therefore confirming the heat source temperatures selected for this study.

Overall, an interesting result of Figure 7 is that this analysis suggests that the same turbine may be utilised within a number of different ORC applications by selecting a suitable working fluid. This allows the same turbine to be produced on a relatively large scale, improving the economic feasibility of the system. When supplied with a specific heat source of a known temperature and mass flow rate, Figure 7 can be used to indicate the most appropriate working fluid that will allow the turbine to operate most effectively, therefore producing the maximum power.

6. Conclusion

This paper has extended work on the development of a radial turbine for low temperature ORC applications by combining a turbine's performance map with a thermodynamic analysis of the cycle. When supplied with a particular heat source temperature, this model has been used to establish the range of heat source mass flow rates that can be effectively converted into power using an ORC that incorporates this existing turbine design. It has been shown that when provided with a particular heat source temperature and working fluid there is an optimal heat source mass flow rate that can be accommodated by this design. This fact has been used to show that the same turbine can be effectively utilised within a range of different ORC applications, simply by changing the working fluid. This is a significant result, since it allows the same turbine design to be produced on a relatively large scale, but implemented into a variety of applications, improving the economy of scale. The results indicate that the examined turbine can be used for heat source temperatures ranging from 360K to 400K, with mass flow rates between 0.45kg/s and 2.7kg/s. The resulting power output ranges between 1.5kW and 27kW, depending on the working fluid selected.

7. Acknowledgement

The authors would like to thank the UK Engineering and Physical Sciences Research Council (EPSRC) for funding this research.

8. References

- [1] Turboden, 2014, "Turboden – Organic Rankine Cycle Turbogenerators for Clean Electric Energy Production", www.turboden.eu, [Accessed: 15/11/2015].
- [2] ORMAT Technologies Inc., 2014, "ORMAT Technologies Inc.", www.ormat.com [Accessed: 15/11/2015].

- [3] Infinity Turbine, 2014, "Infinity Turbine", www.infinityturbine.com, [Accessed: 09/12/2014].
- [4] Electratherm, 2014, "Energy Efficient Green Machine Heat to Power Generation System", www.electratherm.com, [Accessed: 09/12/2014].
- [5] Casati, E., Vitale, S., Pini, M., and Persico, P., 2014, "Centrifugal Turbines for Mini-Organic Rankine Cycle Power Systems", ASME Journal of Engineering for Gas Turbines and Power, **136**(12).
- [6] Lang, W., Colonna, P., and Almbauer, R., 2013, "Assessment of Waste Heat Recovery From a Heavy-Duty Truck Engine by Means of an ORC Turbogenerator", ASME Journal of Engineering for Gas Turbines and Power, **134**(4).
- [7] Bracco, R., Clemente, S., Micheil, D., and Reini, M., 2013, "Experimental tests and modelization of a domestic-scale ORC (Organic Rankine Cycle)", Energy, **58**, pp. 107-116.
- [8] Declaye, S., Quoilin, S., Guillaume, L., and Lemort, V., 2013, "Experimental study on an open-drive expander integrated into an ORC (Organic Rankine Cycle) system with R245fa as working fluid", Energy, **55**, pp. 173-183.
- [9] Leibowitz, H., Smith, I. K., and Stosic, N., 2006, "Cost Effective Smalle Scale ORC Systems for Power Recovery from Low Grade Heat Sources", IMECE2006-14284, Proc. 2006 ASME International Mechanical Engineering Congress and Exposition, Chichago, Illinois, USA.
- [10] Quoilin, S., Van Den Broek, M., Declaye, S., Dewalleg, P., and Lemort, V., 2013, "Techno-economic survey of Organic Rankine Cycle (ORC) systems", Renewable and Sustainable Energy Reviews, **22**, pp. 168-186.
- [11] Chen, H., Goswami, D. Y., and Stefanakos, E. K., 2013, "A review of thermodynamic cycles and working fluids for the conversion of low grade heat", Renewable and Sustainable Energy Reviews, **14**, pp. 3059-3067.
- [12] Saleh, B., Koglbauer, G., and Wendland., M., and Fischer., J., 2007, "Working fluids for low-temperature organic Rankine cycles", Energy, **32**, pp. 1210-1221.
- [13] Tchanche, B. F., Papadakis, G., Lambrinos, G., and Frangoudakis, A., 2009, "Fluid selection for a low-temperature solar organic Rankine cycle", Applied Thermal Engineering, **29**, pp. 2468-2476.
- [14] Rashidi, M. M., Beg, O. A., Parsa, A. B., and Nazari, F., 2011, "Analysis and optimization of a transcritical power cycle with regenerator using artificial neural networks and genetic algorithms", Proceedings of the Institution of Mechanical Engineers, Part A: Journal of Power and Energy, **225**, pp. 701-717.
- [15] Sun, J., and Li, W., 2011, "Operation optimization of an organic rankine cycle (ORC) heat recovery power plant", Applied Thermal Engineering, **31**, 2032-2041.
- [16] Wang, Z. Q., Zhou, N. J., Guo., J., and Wang, X. Y., 2012, "Fluid selection and parametric optimization of organic Rankine cycle using low temperature waste heat", Energy, **40**, 107-115.
- [17] Moustapha, H., Zelesky, M. F., Baines, N. C., and Japiske, D., 2003, *Axial and Radial Turbines*, Concepts ETA, Inc.
- [18] Aungier, R. H., 2006, *Turbine Aerodynamics: Axial-Flow and Radial In-flow Turbine Design and Analysis*, ASME, United States.
- [19] Manente, G., Toffolo, A., Lazzaretto, A., and Paci, M., 2013, "An Organic Rankine Cycle off-design model for the search of the optimal control strategy", Energy, **58**, pp. 97-106.
- [20] Calise, F., Capuozzo, C., Carontenuto, A., and Vanoil, L., 2014, "Thermoeconomic analysis and and off-design performance of an organic Rankine cycle powered by medium temperature heat sources", Solar Energy, **103**, pp. 595-609.
- [21] Li, J., Pei, G., Li, Y., Wang, D., and Ji, J., 2013, "Examination of the expander leaving loss in variable organic Rankine cycle operation", Energy Conversion and Management, **65**, pp. 66-74.
- [22] White, M., and Sayma, A. I., 2015, "System and component modelling and optimisation for an efficient 10kWe low temperature organic Rankine cycle utilising a radial inflow expander", Proceedings of the Institution of Mechanical Engineers, Part A: Journal of Power and Energy, In Press.

- [23] White, M., and Sayma A. I., 2015, "The One-Dimensional Meanline Design of Radial Turbines for Small Scale Low Temperature Organic Rankine Cycles", Proc. GT2015 ASME Turbo Expo: Turbine Technical Conference and Exposition, Montreal, Canada.
- [24] Lemmon, E. W., Huber, M. L., and McLinden, M. O., 2013, "NIST Standard Reference Database 23: Reference Fluid Thermodynamic and Transport Properties-REFPROP", Version 9.1, National Institute of Standards and Technology, Standard Data Program, Gaithersburg.